Available online at www.sciencedirect.com
ScienceDirect
Journal of Hydrodynamics
2009,21(1):1-11
DOI: 10.1016/S1001-6058(08)60112-2
www.sciencedirect.com/science/journal/10016058

NONLINEAR FLUID DAMPING IN STRUCTURE-WAKE OSCILLATORS IN MODELING VORTEX-INDUCED VIBRATIONS*

LIN Li-ming
Division of Engineering Sciences, Institute of Mechanics, Chinese Academy of Sciences, Beijing 100190, China, E-mail: llm@lnm.imech.ac.cn
LING Guo-can
The State Key Laboratory of Nonlinear Mechanics, Institute of Mechanics, Chinese Academy of Sciences, Beijing 100190, China
WU Ying-xiang, ZENG Xiao-hui
Division of Engineering Sciences, Institute of Mechanics, Chinese Academy of Sciences, Beijing 100190, China

(Received April 26, 2008, Revised November 17, 2008)

Abstract: A Nonlinear Fluid Damping (NFD) in the form of the square-velocity is applied in the response analysis of Vortex-Induced Vibrations (VIV). Its nonlinear hydrodynamic effects on the coupled wake and structure oscillators are investigated. A comparison between the coupled systems with the linear and nonlinear fluid dampings and experiments shows that the NFD model can well describe response characteristics, such as the amplification of body displacement at lock-in and frequency lock-in, both at high and low mass ratios. Particularly, the predicted peak amplitude of the body in the Griffin plot is in good agreement with experimental data and empirical equation, indicating the significant effect of the NFD on the structure motion.

Key words: Vortex-Induced Vibration (VIV), Nonlinear Fluid Damping (NFD), wake oscillator

1. Introduction

Vortex-Induced Vibrations (VIV) of structures are of practical interest in many engineering situations, such as bridges and offshore structures, and important in engineering designs as possible large-amplitude oscillations may lead to the potential fatigue of the structures. Therefore, an accurate prediction of peak amplitude of the structure is one of tasks of the study on VIV.

Many studies modelled the fluid/structure interaction with a coupled system. The noteworthy wake oscillator, in which the flow variable is assumed to satisfy the nonlinear van der Pol or Rayleigh equation to simulate the self-sustained dynamic system, was proposed and developed by Birkhoff and Zarantonello[1] and others in describing the dynamics in the near wake. Then the wake/structure interaction is solved by coupling the wake oscillator and structure motion (regarded as the structure oscillator). During the recent decade, many researchers[2,3] adopted such coupled systems in two-dimensional crosswise VIV, or developed spanwisely distributed oscillators in the structure in three-dimensional VIV under complex currents. Some major features of the vortex shedding in the near wake and VIV were described, compared to experiments qualitatively and quantitatively. However, in coupled wake and structure oscillators, the wake patterns related to the different response characters could not be obtained. More complex phenomena in VIV, for instance, the added mass, and the characteristics at low mass-damping parameters, were reviewed by Sarpkaya[4] and Williamson and Govardhan[5].

The vortex-excited oscillation is actually a forced one with a self-excited character to some degree owing to the lift force amplification through nonlinear

* Project supported by the National High Techology Research and Development Program of China (863 Program, Grant No.2006AA09Z350), the Chinese Academy of Sciences (Grant No. KJCX2-YW-L02).
Biography: LIN Li-ming(1977-), Male, Ph. D.

interactions, which are not manifested in the coupled models of structure and wake oscillators currently proposed or used in Ref. [2], such as the fluid damping force and the effects of the structure motion on the near wake dynamics. There are different viewpoints in the fluid force decomposition. Especially, the fluid damping should be proportional to the square of the oscillating velocity of the structure according to its physical nature, while a linear fluid damping is commonly applied in previous studies. In coupled models, the structure oscillator is usually linear with respect to the oscillating amplitude, while the wake oscillator is nonlinear due to the self-excited nature of vortex shedding (as well as the lift force). One of consequences by applying the linear fluid damping is the distinct underestimation of the response amplitude, particularly at a low mass ratio, which will invalidate the prediction of fatigue of the structure in practice. For example, the peak amplitudes in experiments are in the range of (0.5, 1.5), greatly higher than the value 0.25 obtained from the linear fluid damping, at low Skop-Griffin parameters (0.01, 0.1). Therefore, the nonlinear fluid damping related with the square-velocity should be applied, in the meantime, other possible nonlinear interactions may be ignored.

Besides, there are other studies on VIV through numerical simulations[6,7] to build a relationship between wake pattern and structure motion at lock-in. There are also other methods or techniques developed or proposed in order to suppress the vortex shedding[8,9], further the VIV[10].

The main objective of the present study is to investigate the elementary dynamic effect of the nonlinear fluid damping in a coupled system and the underlying physical mechanism. This will help understand the dynamic interaction between the near wake and structure. The simplest physical model of VIV is two-dimensional and one degree-of-freedom elastically supported rigid cylinder with a circular section. The basic van der Pol equation coupled with the structure oscillator with linear and nonlinear fluid dampings is discussed in detail (Section 2). Then, such dynamic systems with different fluid dampings are calculated and compared with experimental data, including the prediction of the peak amplitude (Section 3). In Section 4, discussions are concentrated on the nonlinear fluid damping and corresponding problems. Finally, main results are summarized in Section 5.

2. Physical model of VIV

2.1 *Wake oscillator—van der Pol equation*

Figure 1 shows the schematic diagram of the coupling model of structure and wake oscillators in two-dimensional vortex-induced vibrations. A one degree-of-freedom elastically supported rigid circular cylinder of diameter D is constrained to oscillate transversely (in y-direction) in a steady and uniform incoming flow with velocity U_∞ (in x-direction). As the main feature of the near wake dynamics in the vortex-induced vibration, the alternating vortex shedding is described by the nonlinear self-excited van der Pol equation as

$$\ddot{q} + \varepsilon\Omega_f (q^2 - 1)\dot{q} + \Omega_f^2 q = F_s \tag{1}$$

which is referred to as the wake oscillator[2] and where $(\bullet)$ denotes the derivative with respect to the dimensional time T, q is the the non-dimensional wake variable and ε is damping parameter. The vortex-shedding angular frequency is $f = 2\pi StU_\infty / D$, where St is the Strouhal number. The right-hand side F_s in Eq.(1) is the vibrated structural action on the near wake.

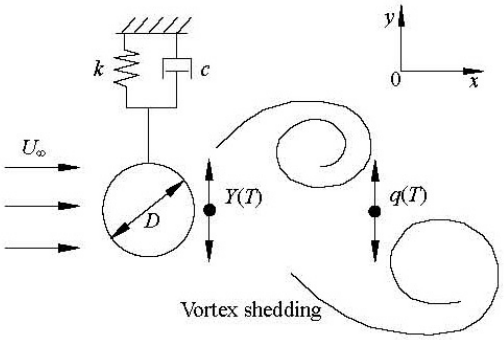

Fig.1 Schematic diagram of the coupling model of structure and wake oscillators in two-dimensional vortex-induced vibrations

2.2 *Structure motion—Linear Fluid Damping* (*LFD*)

The equation of the two-dimensional motion of the body, as a linear oscillator, expressed in the dimensional cross-flow displacement Y, can be written as

$$m_s\ddot{Y} + c_s\dot{Y} + kY = F_f \tag{2}$$

which is referred to as the structure oscillator and where m_s is the structure mass, c_s is the linear structural damping due to the viscous dissipations in the support or the internal friction of the material, and k is the linear spring constant or stiffness related to external effects. The right-hand side F_f in Eq.(2) is the hydrodynamic force on the structure, depending on the amplitude of the lift coefficient. Besides, all mass, damping and stiffness, as well as those defined in the sequel, are defined per unit length.

The fluid force on the structure F_f includes the potential force $F_{potential}(=-m_f\ddot{Y})$, where m_f is the potential fluid-added mass, $m_f = C_a\pi\rho D^2/4$, C_a is the ideal added-mass coefficient and ρ is the fluid density, and the vortex force F_{vortex}, and Facchinetti et al.[2] added the LFD force $F_{DLinear}$ (see Section 2.3) as one of the basic fluid effects. Hence, $F_{DLinear}$ and F_{vortex} are defined as

$$F_{DLinear} = -c_{fLinear}\dot{Y} = -C_D\frac{1}{2}\rho DU_\infty\dot{Y},$$

$$F_{vortex} = C_L\frac{1}{2}\rho DU_\infty^2 \tag{3}$$

where the LFD coefficient $c_{fLinear} = C_D\rho DU_\infty/2$ is defined by means of the drag coefficient on the structure C_D, and C_L is the vortex lift coefficient on the structure, which is different from the classical definition, which amounts to the total lift coefficient C_L^{tot}. It is necessary to include the fluid damping due to the energy dissipation being always proportional to $-\dot{Y}$, if the vortex lift force F_{vortex} is a decomposed component of the total fluid force F_f, or if the body is forced to oscillate in a still fluid. Such fluid damping sometimes is predominant in the decay of the system in still air, particularly at a low mass ratio of the body $m^*(=4m_s/(\pi\rho D^2))$ or mass-damping parameters (discussed in Section 2.4).

Therefore, the structure dynamic motion of Eq.(2) becomes

$$m\ddot{Y} + c\dot{Y} + kY = F_{vortex} \tag{4}$$

where the mass m and damping c include both effects of the structure and fluid,

$$m = m_s + m_f = \mu\rho D^2 \quad , \quad c = c_s + c_{fLinear} \tag{5}$$

and $\mu(=(m^*+C_a)\pi/4)$ is the non-dimensional mass ratio. Now, the natural angular frequency $\Omega_s(=2\pi f_N)$ is defined as $\Omega_s = \sqrt{k/m}$, and the structure reduced damping $\xi = c_s/(2m\Omega_s)$ with c_s as defined in Eq.(5).

2.3 *Modified structure motion—Nonlinear Fluid Damping* (*NFD*)

Generally, the fluid force on the static body is normalized by $\rho DU_\infty^2/2$. For example, the drag force

$$F_D = C_D(Re)\frac{1}{2}\rho DU_\infty^2 \tag{6}$$

where the drag coefficient C_D is dependent upon the Reynolds number, $Re = U_\infty D/\nu$, in which ν is the kinetic viscosity of fluid. Then, for the moving body in the still water with $U_\infty = \dot{Y}$, the drag force becomes nonlinear with respect to the nonlinear damping coefficient $c_{fNonlinear}$ as

$$F_{DNonlinear} = -c_{fNonlinear}\dot{Y},$$

$$c_{fNonlinear} = C_D(Re_s)\frac{1}{2}\rho D\left|\dot{Y}\right| \tag{7}$$

It can also be seen in the so-called "Morison-O'Brien-Johnson-Schaaf" equation. In Eq.(7), the main difference is the drag coefficient measured at the reference Reynolds number, $Re_s = \left|\dot{Y}\right|D/\nu$ (the local Reynolds number), based on the body moving velocity $\left|\dot{Y}\right|$ in Eq.(6).

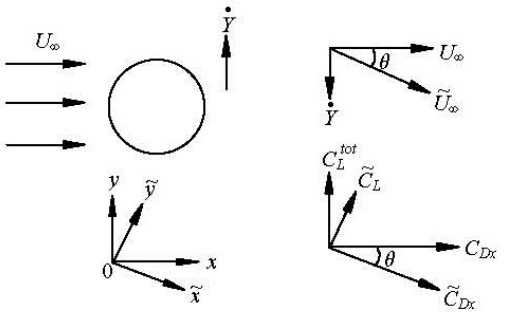

Fig.2 The fluid force on the body with velocity of $\dot{Y}$ moving transversely in the incoming flow U_∞

We now only consider the structure with velocity $\dot{Y}$ moving transversely in the incoming flow U_∞, as shown in Fig.2. Then, as the total velocity of the oscillated cylinder, the "effective " incoming flow $\tilde{U}_\infty$, inclined with respect to the *x*-direction with angle θ, would be

$$\tilde{U}_\infty = \sqrt{U_\infty^2 + \dot{Y}^2} = U_\infty\sqrt{1+\tan^2\theta},$$

$$\theta = \arctan\left(\frac{\dot{Y}}{U_\infty}\right) \tag{8}$$

And "effective" fluid forces, denoted by "vertical" lift coefficient $\tilde{C}_L$ and "streamwise" drag coefficient $\tilde{C}_{Dx}$ (also inclined with respect to the x direction with θ) on the cylinder in the oscillating coordinates $(\tilde{x},\tilde{y})$ are related with fluid forces, denoted by C_L^{tot} and C_{Dx}, in the normal Cartesian coordinates (x,y) as

$$F_L = \tilde{F}_L + \tilde{F}_{Dx} = C_L^{tot}(\widetilde{Re})\frac{1}{2}\rho D\tilde{U}_\infty^2 =$$

$$\left[\tilde{C}_L(\widetilde{Re})\cos\theta\right]\frac{1}{2}\rho D\tilde{U}_\infty^2 -$$

$$\left[\tilde{C}_{Dx}(\widetilde{Re})\sin\theta\right]\frac{1}{2}\rho D\tilde{U}_\infty^2 =$$

$$\left(\tilde{C}_L U_\infty - \tilde{C}_{Dx}\dot{Y}\right)\frac{1}{2}\rho D\tilde{U}_\infty =$$

$$\tilde{C}_L\frac{1}{2}\rho DU_\infty\tilde{U}_\infty - \tilde{C}_{Dx}\frac{1}{2}\rho DU_\infty\dot{Y}\bullet$$

$$\sqrt{1+\tan^2\theta} \tag{9}$$

C_L and $\tilde{C}_{Dx}$ are obviously correlated with the total Reynolds number $\widetilde{Re} = \tilde{U}_\infty D/\nu$ and the angle θ. From Eq.(9), the transverse force F_L is made up of two components due to the "vertical" lift $\tilde{F}_L$ and "streamwise" drag $\tilde{F}_{Dx}$. In a sense, the magnitude of drag, depending on the oscillating motion, can be taken into account in the form of $\tilde{C}_{Dx}\sqrt{1+\tan^2\theta}$ if the LFD in the second term at the right-hand side of Eq.(9) is assumed.

For simplicity, if $\left|\dot{Y}(T)\right| \ll U_\infty$ and $\tilde{C}_L$ are independent of oscillating angle θ [11] in VIV and then $\tilde{U}_\infty \approx U_\infty$ or $\widetilde{Re} \approx Re$, the force components $\tilde{F}_L$ and $\tilde{F}_{Dx}$ in Eq.(9) are reduced to

$$\tilde{F}_L \approx \tilde{C}_L(Re)\frac{1}{2}\rho DU_\infty^2,$$

$$\tilde{F}_{Dx} \approx -\tilde{C}_{Dx}(Re)\frac{1}{2}\rho DU_\infty\dot{Y} \tag{10}$$

Compared to Eq.(9), the lift force $\tilde{F}_L$ still plays an important and dominant role in the induced vibration of the body. Meantime, the added drag force $\tilde{F}_{Dx}$ is a small increment to the excited fluid force due to the body oscillation, which is linear with respect to the oscillating velocity $\dot{Y}$.

Furthermore, in a comparison between Eqs.(7) and (10), if they could be treated as the fluid damping, we may see two main differences: (1) $C_D(Re_s)$ and $\tilde{C}_{Dx}(Re)$ are given at the vertical and streamwise directions, following different physical mechanisms, such as the pressure difference in *y*-direction and in *x*-direction because of the small contribution of viscous components in drag, (2) correspondingly, the reference Reynolds numbers in the measurement of drag coefficients are Re_s and Re, respectively. With the above assumption of $\left|\dot{Y}\right| \ll U_\infty$, we have $Re_s \ll Re$. It seems that we will have

$$C_D(Re_s)\left|\dot{Y}\right| \simeq \tilde{C}_{Dx}(Re)U_\infty \tag{11}$$

which may be taken as a hypothesis without any proof if the LFD is applied. And in Eq.(11), we will have

$$\frac{C_D(Re_s)}{\tilde{C}_{Dx}(Re)} \sim \frac{U_\infty}{\left|\dot{Y}\right|} \gg 1 \tag{12}$$

Such relationship, if applied in the fixed circular cylinder, is reliable because the drag coefficients are high ($\propto Re^{-1}$, e.g. $C_D(Re_s)$) at low Reynolds numbers ($<10^2$) but are getting lower (~1.0, e.g. $\tilde{C}_{Dx}(Re)$) at higher Reynolds numbers (10^2 ~ 3×10^5). Besides, it is also noted that the linearity for the drag at low velocities, different from that in Eq.(3), is adopted as $C_D \propto Re^{-1}$.

In this way, the LFD, Eq.(3), is employed only under the assumption that $\left|\dot{Y}\right| \ll U_\infty$. Otherwise, the prediction based on the LFD, Eq.(3), may be greater by at least one order of magnitude than that based on nonlinear one, Eq.(7), which would underestimate the oscillating amplitude of the body and further influence the dynamic behaviors. This situation may occur when $C_D(Re_s) \sim \tilde{C}_{Dx}(Re) \sim 1.0$, such as for a free cable oscillation at high velocity $\dot{Y}$, where Re_s and Re

are all greater than 100. On the other hand, the nonlinear fluid damping also can be joined in the total fluid force as an independent fluid effect on the structure (see in Section 2.2), if the structure oscillator Eq.(4) with the vortex lift force is applied. Consequently, it is reasonable to adopt the NFD, Eq.(7), in the structure oscillator Eq.(4), in which the damping coefficient is $c = c_s + c_{fNonlinear}$. It should be also noticed that the reference velocity U_∞ in Eq.(6) is replaced by the oscillating velocity $\dot{Y}$, rather than the relative velocity considering the vertical velocity of fluid near the cylinder. As we know now, in the vortex dynamics for the cylinder wake, the increase in Reynolds numbers is associated with a sequence of fundamental shear flow instabilities: wake transition, shear layer transition and boundary layer transition. And the shear-layer transition regime is correspondingly in the range of Reynolds numbers (10^3, 2×10^5). Based on this fact, despite the fact that the transition of the free shear layer could be developed due to the Kelvin-Helmholtz instability or else, the boundary or shear layer closely around the cylinder can be assumed to be in the laminar state without transition. The fluid within such region will move with the oscillating cylinder at the same velocity, as suggestted by the potential force component $F_{potential}$. The fluid outside such region, except for the shedding vortex resulting in the "vortex force" F_{vortex}, with a neglectfully small vertically oscillating velocity as compared with $\dot{Y}$, mainly affects the body's vibration through the fluid damping. Thus U_∞ could be approximately replaced by $\dot{Y}$.

2.4 *Coupled dynamic system*

Based on the structure and wake oscillators, Eqs.(1) and (4), and by introducing the dimensionless displacement $y = Y/D$ and time $t = T\Omega_f$, the nondimensional coupled system with the NFD Eq.(7) becomes

$$\ddot{y} + 2\xi\delta\dot{y} + \frac{C_D(Re_s)}{2\mu}|\dot{y}|\dot{y} + \delta^2 y = f \tag{13a}$$

$$\ddot{q} + \varepsilon(q^2 - 1)\dot{q} + q = s \tag{13b}$$

where $(\bullet)$ means the derivative with respect to t. For the convenience of comparison between results obtained from the linear and nonlinear fluid dampings, the dimensionless structure-fluid coupling system with the LFD[2], Eq.(3), is also given as

$$\ddot{y} + \left[2\xi\delta + \frac{C_D(Re)}{4\pi St\mu}\right]\dot{y} + \delta^2 y = f \tag{14a}$$

$$\ddot{q} + \varepsilon(q^2 - 1)\dot{q} + q = s \tag{14b}$$

In Eqs.(13) or (14), the reduced ratio of angular frequency of the structure δ is related to the reduced flow velocity U_r by

$$\delta = \frac{\Omega_s}{\Omega_f} = \frac{\Omega_s}{\frac{2\pi StU_\infty}{D}} = \frac{1}{StU_r},\ U_r = \frac{2\pi}{\Omega_s}\frac{U_\infty}{D} \tag{15}$$

with respect to the wake variable q, since the excited fluid force on the right-hand side of Eq.(4) is interpreted as the vortex force, Eq.(3), the wake oscillator is solved for the vortex lift coefficient C_L, which is also varied with time t. Hence, q is defined as a reduced vortex lift coefficient $q = 2C_L/C_{L0}$, where the reference lift coefficient C_{L0} is that observed on a fixed body due to vortex shedding. Then, the dimensionless coupling force term for the structure oscillator is given as

$$f = \frac{F_{vortex}}{mD\Omega_f^2} = Mq,\ M = \frac{C_{L0}}{16\pi^2 St^2\mu} \tag{16}$$

in which M serves as a mass number and scales the effect of the vortex motion on the structure.

The influence F_s of the oscillating structure on the wake in Eq.(1) is non-dimensionalized as $s = F_s/(D\Omega_f^2)$ in Eq.(13). Three coupling models proposed in literature[2,12] are: displacement coupling $s = Ay$, velocity coupling $s = A\dot{y}$ and acceleration coupling $s = A\ddot{y}$, respectively, where A is a parameter[13,14]. In Facchinetti et al.[2], it is shown that the best qualitative and quantitative agreement with experimental data is achieved in the acceleration model. Then, the acceleration model is employed in the present study.

Moreover, in literature[3], the structural damping is usually neglected. Here the damping ratio α of fluid damping c_f to structural damping c_s is introduced to see why one may ignore c_s, $\alpha = c_f/c_s$. In models with LFD and NFD, damping ratios are

$$\alpha_{Linear} = \frac{c_{fLinear}}{c_s} = \frac{C_D(Re)}{8\pi St\mu\xi\delta} = \frac{C_D(Re)U_r}{8\pi\mu\xi} \quad (17a)$$

$$\alpha_{Nonlinear} = \frac{c_{fNonlinear}}{c_s} = \frac{C_D(Re_s)|\dot{y}|}{4\pi\mu\xi\delta} = \frac{C_D(Re_s)|\dot{y}|StU_r}{4\pi\mu\xi} \quad (17b)$$

where the product of μ and ξ is defined as the total mass-damping parameter, $\mu\xi$, as is different from the (structural) mass-damping parameter, $m^*\xi$. From Eq.(17), it is clear that the condition for neglecting c_s is a high reduced velocity U_r, or a low total mass-damping $\mu\xi$. As will be discussed later on, it is necessary to estimate $\alpha_{Nonlinear}$ to evaluate the oscillating velocity $\dot{y}$ varied with time. Assume a constant damping coefficient $C_D(Re_s)$ and a harmonic solution $y(t) = y_0\sin(\omega t)$ with the time-averaged amplitude of oscillation y_0 and the amplification of angular frequency ω for simplicity, the nonlinear damping ratio $\alpha_{Nonlinear}$ could be simply evaluated by the time-averaged velocity $\overline{|\dot{y}|}$ in one period of $T_y(=2\pi/\omega)$ as

$$\bar{\alpha}_{Nonlinear} = \frac{C_D\overline{|\dot{y}|}}{4\pi\mu\xi\delta} = \frac{C_D y_0}{\pi\mu\xi\delta T_y} = \frac{C_D y_0\omega}{2\pi^2\mu\xi\delta} \quad (18)$$

This shows that the time-averaged effect of fluid damping would be greater than that of structure damping in VIV with larger amplitude y_0. Particularly, at the lock-in with $\delta = \omega = 1$, Eqs.(17a) and (18) yield

$$\alpha_{Linear0} = \frac{C_D}{8\pi St\mu\xi} \quad (19a)$$

$$\bar{\alpha}_{Nonlinear0} = \frac{C_D\, y_0|_{\delta=1}}{2\pi^2\mu\xi} \quad (19b)$$

3. Dynamic analysis of the coupled system

3.1 *Parameters and numerical methods*

All basic parameters used in the coupled dynamic system, such as St, C_a, and so on, are the same as used in Ref.[2], $St = 0.2$, $C_a = 1$, $C_{L0} = 0.3$. As mentioned there, the assumption of St being a constant is commonly used in the sub-critical range, $300 < Re < 1.5\times10^5$.

Some parameters are determined only in some special cases in order to compare numerical results with experiments, like μ, ξ, $C_D(Re)$. However, the assumption that the NFD is equal to a constant amplified drag coefficient for comparison, $C_D(Re_s) = C_D(Re) = 2.0$ [2,11], is adopted in a certain range, Re_s, $Re > 300$.

Parameters of A and ε are the same as used by Facchinetti et al.[2], $A = 12$ and $\varepsilon = 0.3$, because their determination is independent of whether a linear or nonlinear fluid damping model is adopted, even independent of the structure oscillator.

Two coupling systems are discretized explicitly for the LFD and implicitly for the NFD by a standard centered finite difference in time with a second order. The time step is chosen in order to achieve stability, $\Delta t = 0.01$, which is also used in the following parts.

3.2 *Comparison between two dynamic systems*

In this subsection, numerical results obtained from the dynamic system with the LFD, Eq.(14), are presented, and compared with those with the NFD, Eq.(13). The case is calculated at a high mass-ratio $\mu = 250$ ($M \approx 2\times10^{-4}$ and $m^* = 317.3$) and the structure reduced damping $\xi = 0.0031$. Characteristics of response at lock-in are mainly investigated in four aspects: (1) the nondimensional frequency ratio f^* of the structural oscillation frequency, f_s, to the natural frequency in fluid $f_N(=(2\pi)^{-1}\Omega_s)$, $f^* = f_s/f_N$, (2) the vortex shedding frequency of the body in motion, f_f, non-dimensionalized by the vortex shedding frequency of the body at rest $f_{v0}(=(2\pi)^{-1}\Omega_f)$, f_f/f_{v0}, (3) the time-averaged amplitude of oscillation of the body y_0, (4) the time-averaged amplitude of wake variable q_0.

As shown in Fig.3, the main dynamic features of the coupled system with the NFD, Eq.(13), are qualitatively consistent with those with the LFD, Eq.(14). The oscillating frequency of the body is synchronized onto the vortex shedding frequency in Strouhal law at lock-out, as predicted by the theory of the linear vibration, whereas at lock-in the response of the body and vortex shedding is characterized by the frequency near the natural frequency of the body in still fluid and by hysteresis phenomenon at both lock-in boundaries, see in Figs.3(a) and 3(b). Outside the lock-in region, the response amplitude is very

small, $y_0 \ll 1$, indicating that the body is almost at rest (here we set $y_0 \sim O(10^{-3})$). At lock-in, the magnification of oscillating amplitude is also determined, as well as the vortex lift force.

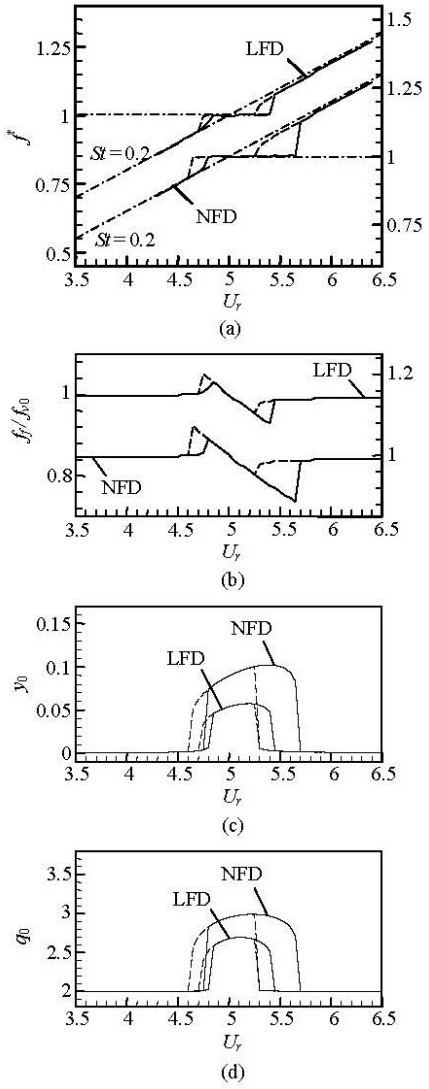

Fig.3 Comparison of coupled systems with the NFD to that with the LFD in (a) f^*, (b) f_f / f_{v0}, (c) y_0 and (d) q_0 as a function of U_r: —— increasing U_r, – – – decreasing U_r. Note that values of left- or right-*y*-axis in (a) and (b) are related to models with the linear or nonlinear fluid dampings, respectively, and the data in (a) are selected only when $y_0 > O(10^{-3})$ since the body is almost at rest

The primary difference between these two dynamic systems in this case is that the range of reduced velocity U_r at lock-in in the NFD model is greater than that in the LFD model, so are the amplitudes of body oscillation and vortex lift. The mechanisms responsible for such quantitative difference are: (1) the subordinate effect of the fluid damping, as compared with the structure damping, on structural motions $y_0|_{\delta=1} \approx 0.09$, and (2) the NFD is much weaker than the LFD. This could be estimated quantitatively by Eq.(19). In this case at a high mass ratio, $\alpha_{Linear0} = 0.513$ and $\alpha_{Nonlinear0} \approx 0.01$ ($y_0|_{\delta=1} \approx 0.09$, see Fig.3(c)). Therefore, as stated above, the fluid damping, whether in the linear or nonlinear model, will affect the coupled system obviously in the case of small mass ratio or mass-damping parameter (see also the next subsection).

3.3 *Comparison between numerical and experimental results*

First, the prediction of the maximum amplitude of the oscillating body in the Griffin plot is used, although the related dynamic system is two-dimensional. The Griffin plot is generally used in establishing the relationship between the maximum response amplitude $y_{0\max}$ at lock-in and the combined response parameter termed S_G [15], defined as $S_G = 2\pi^3 St^2 (m^* \xi)$. According to the assumption that the solution of Eq.(14) is harmonic and the high-frequency component in the wake oscillator can be ignored[2], the maximum structure displacement amplitude $y_{0\max}$ is explicitly related with $S_{G\mu}$ based on the total mass-damping parameter, $S_{G\mu} = 8\pi^2 St^2 (\mu\xi)$, at lock-in $\omega = \delta = 1$ and $U_r = St^{-1}$,

$$y_{0\max} = \frac{\frac{C_{L0}}{2}}{S_{G\mu} + \pi St C_D} \sqrt{1 + \frac{A}{\varepsilon} \frac{\frac{C_{L0}}{4}}{S_{G\mu} + \pi St C_D}} \qquad (20)$$

The parameters used in computation are classified into two kinds: (1) special cases in experiments, $m^* = 248$ and $\xi = 0.00103$ [16], $m^* = 10.3$ and $\xi = 9.7 \times 10^{-4}$, $m^* = 8.63$ and $\xi = 0.00151$, $m^* = 1.19$ and $\xi = 0.00502$, and $m^* = 0.52$ and $\xi = 0.0052$ [17], (2) series of mass-damping parameters, $(m^* + C_a)\xi = 0.005$, 0.01, 0.03, 0.08, 0.1, 0.3, 0.8, 1, 5 with $\xi = 0.003$ falling into the range of most experiments, similar to Newman and Karniadakis[6] with the different ξ and given $m_s/(\rho D^2) (= \pi m^*/4)$. As for the latter, by suggestion of Williamson and Govardhan[5], the data from diverse experiments appear to give a good approximate functional relationship between $y_{0\max}$ and $(m^* + C_a)\xi$ over a wide range of parameters:

$m^* > 2$, $(m^* + C_a)\xi > 0.006$. Hence, the plot of response amplitude versus $(m^* + C_a)\xi$ can be obtained as(see Fig.4(b)).

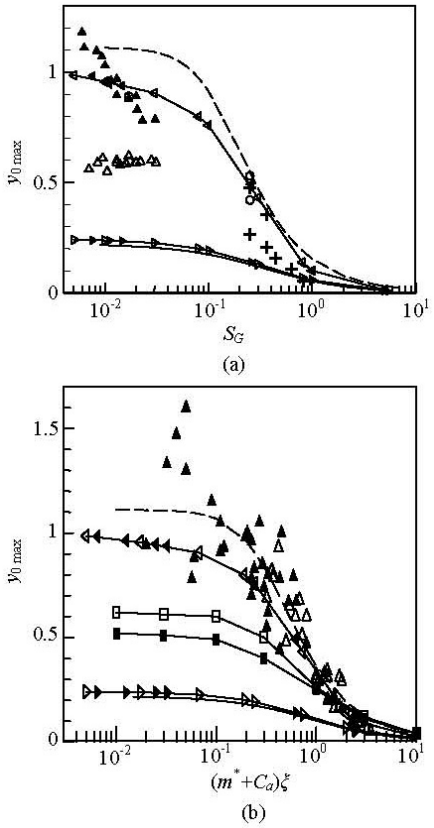

Fig.4 The response amplitude $y_{0\max}$ versus (a) S_G and (b) $(m^* + C_a)\xi$ in the Griffin plot. Common symbols in (a) and (b) are: —— Eq.(20), – – – Eq.(21) with best-fit $B = 0.385$ and $C = 0.12$, –▷– and ►, the LFD model, –□– and ◄, the NFD model. In (a), Δ and ▲, experimental data of Skop and Balasubramanian[18] in air and water, –□– and –■– DNS of Newman and Karniadakis[6] at $m_s/(\rho D^2) = 1$ and 10 at $Re = 100$. In (b), experimental data: + Feng[16], Δ and ▲ Khalak and Williamson[19] for lower and upper branches, ○ Govardhan and Williamson[17]

From Fig.4, the prediction of the response amplitude obtained by the coupled system with the NFD is closer to experimental data than that obtained from DNS at $Re = 100$ or by the coupled system with the LFD, especially at small mass-damping or Skop-Griffin parameters. This difference between the LFD and NFD can only explained by the weaker contribution of the NFD, than that of the LFD, on the structural motion, especially at small mass ratios, despite of the fact that the structure damping is weaker than the fluid damping. In studies on low mass-damping[19], three branches in peak-amplitude are identified as Initial, Upper and Lower branches. Figure 4(b) shows that $y_{0\max}$ is more compatible with that in Upper branch at the low mass-damping. At higher values of $(m^* + C_a)\xi$ or S_G (such as > 1.0), all numerical and experimental data nearly converge together due to the weak contribution of fluid damping. Moreover, a comparison is also made with the empirical equation proposed by Sarpkaya[20] as

$$y_{0\max} = \frac{B}{\sqrt{C + S_G^2}} \tag{21}$$

where constants B and C are 0.385 and 0.12, respectively, obtained through curve fitting[5]. Figure 4 shows that the peak amplitudes of the structure obtained from the NFD model are also in good agreement with Eq.(21) qualitatively and quantitatively with the greatest deviation of less than 20% for low mass-damping, better than those obtained from the LFD model, which further confirms the significance of the NFD in the structure response.

Let us now consider dynamic behaviors of the coupled system at a very small mass ratio, below the critical mass ratio $m^*_{crit} = 0.542$ introduced by Govardhan and Williamson[17]. The computational parameters are $m^* = 0.52$ and $\xi = 0.0052$ [2,17]. And, $\alpha_{Linear0} = 64.1$, $\overline{\alpha}_{Nonlinear0} = 11.1$, indicating that the fluid damping is stronger than that in the cable case.

In experiments, the range of lock-in at such low mass ratio would be quite different from that observed at higher mass ratio. As the structure mass m_s decreases, so the regime of reduced velocity U_r with large-amplitude response increases. The vibration frequency increases almost linearly as U_r increases, without the hysteresis phenomenon, as shown in Fig.5(a), in the limits of experimental facilities. And large-amplitude vigorous vibrations suddenly appear and persist up to an infinite U_r as the mass ratio is reduced to below $m^*_{crit} = 0.542$ (see in Fig.5(b)). In this sense the cylinder resonates forever.

The responses simulated by the LFD and NFD models show that the cylinder will oscillate forever with increasing U_r . In Fig.5(a), both models with the LFD and NFD predict that the oscillation frequency is synchronized at lock-in and increases infinitely at higher U_r , but with different slopes. The coupled system with the LFD is more consistent with experimental data than that with the NFD at a low U_r (such as (3, 5)), after which they all deviate from experimental data. As the regime of lock-in persists up to higher U_r , the response amplitude in the NFD

model increases first along with the experimental data, then drops dramatically from nearly 1 down to 0.2, inconsistent with the LFD model and experimental data qualitatively and quantitatively, as shown in Fig.5(b). The mechanism for this is so far unclear, which may be due to the contribution of fluid damping relative to the linear elastic force $\delta^2 y$ in Eqs.(13) and (14), as can be seen by a simple comparison between two coupled systems. For example, at $U_r = 10$ and 20, the fluid damping in Eq.(13a) reaches the same magnitude of the elastic force of about $O(10^{-1})$ and $O(10^{-2})$, respectively, while the LFD in Eq.(14a) is greater by about one order of magnitude than the elastic force. To some extent, this means that a light structure is oscillating in a very viscous fluid at a high incoming velocity, as illustrated by the LFD model at this mass ratio. Of course, the response amplitude is quite limited.

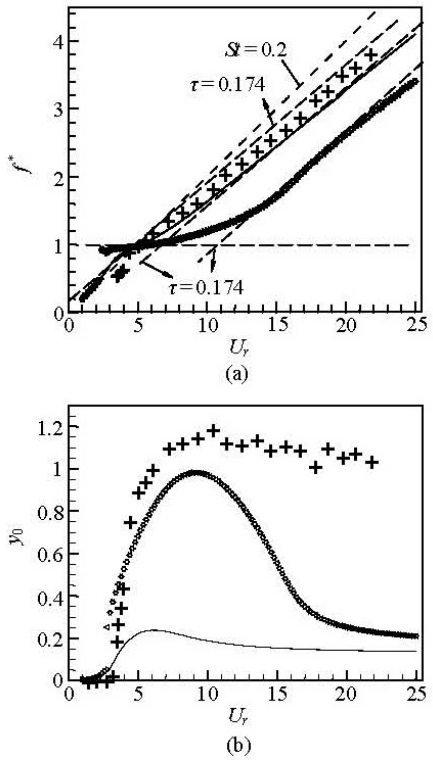

Fig.5 Response characters of (a) f^* and (b) y_0 at the mass ratio $m^* = 0.52$ below the critical value[17], and $\xi = 0.0052$. + experimental data from Govardhan and Williamson[17], ——model with the LFD, ▷ (increasing U_r) and ◁ (decreasing U_r), model with the NFD. τ is the slope of f^*, and 0.174 is from the experimental result[17]

Besides, other features of response can be observed in comparison with experimental data. It is noted in Fig.5(b) that the maximum amplitude in the NFD model appears at about $U_r = 2St^{-1} = 10$ as observed in experiment, rather than at points slightly higher than $U_r = St^{-1} = 5$ as indicated by the LFD model. And the lack of hysteresis phenomenon is also observed with the increasing and decreasing U_r, as shown in Fig.5.

We may therefore conclude that for the coupled system with the NFD to predict the peak amplitude of the structure quantitatively and qualitatively, particularly, at very low mass ratio m^*, one still has some way to go, as well as that with the LFD, albeit some features of VIV can be described.

4. Discussion

According to the above simple comparison between coupled systems with the NFD and LFD, the effects of the NFD on the VIV response are significant at same values of parameters, especially at low mass ratios. With the assumption of drag coefficient $C_D(Re_s) = 2.0$, the NFD leads to a greater increase of oscillating amplitude and velocity of the structure, such as at $m^* = 0.52$ (in Section 3.3), $y_0 = 0.682$ and $|\dot{y}|_{\max} = 0.667$ at $U_r = 5$, whereas $y_0 = 0.221$ and $|\dot{y}|_{\max} = 0.222$ with the LFD. The fluid damping is estimated to be 0.373 by the nonlinear relationship, but 0.148 by the linear expression. It can be argued that the difference of fluid damping with the linear and nonlinear relationships would not be as large as stated above. However, the obvious conclusion is that the higher amplitude will follow with higher oscillating velocity. This can be explained from the energy considerations. As the near wake variable q is directly related to the vortex lift coefficient C_L, the energy transfer from the wake to the structure can be expressed by $\int q\dot{y}\mathrm{d}t$, approximately equal to qy_0 if with a constant lift force q. Then the kinetic energy of the structure $\frac{1}{2}m_s\dot{y}^2$ would be higher as the wake energy input increases with higher y_0. And, the assumption of $|\dot{y}| \ll 1$ applied in Eq.(3) and models does not hold true, especially for the LFD model.

Now let us discuss the assumption of $C_D(Re_s)$ itself used in the present study. As the drag coefficient is varied with different local Reynolds number Re_s and directly related to the oscillating velocity $|\dot{y}|$, the constant assumption in the oscillating process in VIV would seem questionable. In marine engineering, the approximately estimated Re falls into, at least, the range of magnitude $O(10^5 \sim 10^6)$, if $U_\infty \sim O(1)$,

$D \sim O(10^{-1} \sim 1)$ and $\nu \sim O(10^{-6})$. The maximum velocity $\left|\dot{Y}\right|_{\max} \sim O(10^{-3} \sim 10^{-2})U_\infty$ at high mass ratio, where the oscillating velocity would be lower than that at a lower mass ratio, so Re_s would be at least $O(10^{-3})Re$. For a circular-section cylinder, the drag coefficient is nearly constant of 1.0 at the Reynolds number greater than 100. So the constant assumption of C_D is reasonable.

On the other hand, if the variation of the drag coefficient with the time due to $\left|\dot{Y}(T)\right|$ should be considered at certain conditions, the following relationships[11] in a fixed cylinder can be applied in estimating the drag coefficient used in the simulation:

$$C_D(Re_s) = \frac{8\pi}{Re_s(2.002 - \ln Re_s)},\ Re_s < 1 \qquad (22a)$$

$$C_D(Re_s) = 1.3 + \frac{10}{Re_s},\ Re_s \in (1, 10^4) \qquad (22b)$$

The minimum truncation at $Re_s \approx 0$ needs to be performed with $C_D(Re_s) = 0$ when $\left|\dot{Y}(T)\right| (\ll U_\infty)$ is about $O(10^{-3})U_\infty$, or $Re_s \approx O(10^{-2})$. To some extent, the latter criterion of truncation is difficult to realize because $Re_s|_{\min} \sim O(10^{-1})$ if keeping St constant at the range $Re \sim O(10^2 \sim 10^5)$.

Furthermore, from the definitions of the LFD and NFD, Eqs.(10) and (7), and their different physical mechanisms, it seems that there exist two kinds of fluid drag force. The linear one is stemmed from the streamwise drag independent of the oscillating transverse lift, with the pressure difference in *x*-direction disturbed along *y*-direction by the oscillation as the main contribution, while the nonlinear one is stemmed from the transverse drag dependent on the oscillating total lift, also with the pressure difference in *y*-axis as the main contribution, but with a little modification to the transverse lift resulting from the oscillating motion in the real fluid. When the streamwise incoming flow and the transverse oscillating velocity of the structure are independent, the nonlinear fluid damping is reasonable. However, if the compound velocity (see in Fig.2 and Eq.(9)) is considered, there still exists an unknown relationship between the "effective" fluid forces and the oscillating angle. Especially for a free cable with high oscillating velocity, the assumption ($\left|\dot{Y}\right| \ll U_\infty$) does not hold true and consequently Eq.(9) is unsuitable in practical simulations. Therefore, the fluid force on the body for the LFD and NFD models are decomposed and rewritten in crosswise VIV as

$$F_{f\_LFD} = C_L^{tot}\frac{1}{2}\rho D\tilde{U}_\infty^2 = C_L\frac{1}{2}\rho DU_\infty^2 - C_D(Re)\frac{1}{2}\rho DU_\infty\dot{Y} - C_a\frac{\pi}{4}\rho D^2\ddot{Y} \qquad (23)$$

$$F_{f\_NFD} = C_L^{tot}\frac{1}{2}\rho D\tilde{U}_\infty^2 = C_L\frac{1}{2}\rho DU_\infty^2 - C_D(Re_s)\frac{1}{2}\rho D\left|\dot{Y}\right|\dot{Y} - C_a\frac{\pi}{4}\rho D^2\ddot{Y} \qquad (24)$$

It is shown that NFD is effective for prediction of peak amplitude of the structure, which can also be obtained by varying wake parameters A and ε to fit experimental data, as suggested by Facchinetti et al.[2]. For example, if $A = 120$ or $\varepsilon = 0.03$, $y_0|_{\delta=1} = 0.126$ or 0.122 at $\mu = 250$ (in Section 3.2), respectively, while at $m^* = 0.52$ (in Section 3.3), $y_0|_{\delta=1} = 0.628$ or 0.592, respectively, by the coupled system with the LFD, also indicated by Eq.(20). The physical explanations are: (1) increasing A means increasing the structural force on the near wake, resulting in a greater amplification of vortex lift force, such as if $A = 120$, $C_L = 0.853$ at $\mu = 250$ and $C_L = 1.39$ at $m^* = 0.52$, (2) decreasing the van der Pol parameter ε means decreasing the fluid viscous dissipation. Correspondingly, A/ε would be high[2]. But if the total lift magnification factor in the acceleration coupling model is used, A/ε should be small in order to fit experimental data[2]. Consequently, the obvious conflicting consideration is whether A/ε should be greater or smaller. From our point of view, parameters A and ε are not universal constants. Another approach to reduce the discrepancy between the numerical prediction and experimental data is to take the intrinsic three-dimensional factors into account in the simulation of VIV, as proposed by Newman and Karniadakis[6].

5. Conclusions

Due to the limitation of the LFD with the assumption of a low oscillating motion of the body, the NFD is proposed and applied based on the physical definition. The dynamic system is described by the wake oscillator, the van der Pol equation, with the acceleration model coupled with the structure oscillator. The hydrodynamic effect of the NFD on the

two-dimensional VIV is investigated and compared with that of the LFD in response characteristics at very high and low mass ratios. Furthermore, the predictions of the response amplitude of the structure are made for a series of parameters adopted in previous experiments. The detailed investigation into two dynamic systems with these parameters will be carried out in future, in order to find out advantages and disadvantages in describing the complex phenomena in VIV. The conclusions of the present study are as follows:

(1) The NFD in the form of square-velocity relationship can be applied in the structure-wake oscillators as an independent fluid effect for the vortex lift and potential added-fluid force.

(2) At a high mass ratio, the dynamic system with the NFD is similar to that with the LFD qualitatively, only different in a wider lock-in regime, a wider hysteresis loop, a greater amplification of response amplitude and vortex lift force, due to the weak influence of the fluid damping on the structure oscillation.

(3) At a very low mass ratio below the critical value, the model with the NFD can succesfully simulate some dynamic features in VIV quantitatively and qualitatively, as that with the LFD in most cases.

(4) The NFD model can predict the response amplitude in VIV very well, compared well with experimental data and empirical equation, better than the model with the LFD with the same values of parameters.

References

[1] BIRKHOFF G., ZARANTONELLO E. H. **Jets, wakes and cavities**[M]. New York: Academic Press, 1957.

[2] FACCHINETTI M. L., LANGRE E. de and BIOLLEY F. Coupling of structure and wake oscillators in vortexinduced vibrations[J]. **Journal of Fluids and Structures,** 2004, 19: 123-140.

[3] VIOLETTE R., LANGRE E. de and SZYDLOWSKI J. Computation of vortex-induced vibrations of long structures using a wake oscillator model: Comparison with DNS and experiments[J]. **Computers and Structures,** 2007, 85: 1134-1141.

[4] SARPKAYA T. A critical review of the intrinsic nature of vortex-induced vibrations[J]. **Journal of Fluids and Structures,** 2004, 19: 389-447.

[5] WILLIAMSON C. H. K., GOVARDHAN R. Vortex-induced vibrations[J]. **Annual Review of Fluid Mechanics,** 2004, 36: 413-455.

[6] NEWMAN D. J., KARNIADAKIS G. E. A direct numerical simulation study of flow past a freely vibrating cable[J]. **Journal of Fluid Mechanics,** 1997, 344: 95-136.

[7] SHA Yong, WANG Yong-xue. Vortex induced vibrations of finned cylinders[J]. **Journal of Hydrodynamics,** 2008, 20(2): 195-201.

[8] DENG Jian, SHAO Xue-ming and REN An-lu. Vanishing of three-dimensionality in the wake behind a rotationally oscillating circular cylinder[J]. **Journal of Hydrodynamics, Ser. B,** 2007, 19(6): 751-755.

[9] LING Guo-can, LIN Li-ming. A note on the numerical simulations of flow past a wavy square-section cylinder[J]. **Acta Mechinaca Sinica,** 2008, 24(1): 101-105.

[10] LOU Min, GUO Hai-yan and DONG Wen-yi. Suppression of vortex-induced vibration by impact excitation[J]. **Journal of Hydrodynamics, Ser. A,** 2007, 22(4): 508-511(in Chinese).

[11] BLEVINS R. D. **Flow-induced vibrations**[M]. New York: Van Nostrand Reinhold, 1990.

[12] KRENK S., NIELSEN S. R. K. Energy balanced double oscillator model for vortex-induced vibrations[J]. **ASCE Journal of Engineering Mechanics,** 1999, 125(3): 263-271.

[13] MUREITHI N. W., KANKI H. and NAKAMURA T. Bifurcation and perturbation analysis of some vortex shedding models[C]. **Proceedings of the Seventh International Conference on Flow-Induced Vibrations.** Luzern, Switzerland, 2000, 61-68.

[14] PLASCHKO P. Global chaos in flow-induced oscillations of cylinders[J]. **Journal of Fluids and Structures,** 2000, 14: 883-893.

[15] SKOP R. A. On modelling vortex-excited oscillations[R]. Naval Research Laboratory Memorandum Report 2927, 1974.

[16] FENG C. C. The measurements of vortex induced efficts in flow past stationary and oscillating circular and D-section cylinders[D]. Master Thesis, Vancouver, Canada: The University of British Columbia, 1968.

[17] GOVARDHAN R., WILLIAMSON C. H. K. Modes of vortex formation and frequency response of a freely vibrating cylinder[J]. **Journal of Fluid Mechanics,** 2000, 420: 85-130.

[18] SKOP R. A., BALASUBRAMANIAN S. A new twist on an old model for vortex-excited vibrations[J]. **Journal of Fluids and Structures,** 1997, 11: 395-412.

[19] KHALAK A., WILLIAMSON C. H. K. Motions, forces and mode transitions in vortex-induced vibrations at low-mass damping[J]. **Journal of Fluids and Structures,** 1999, 13: 813-851.

[20] SARPKAYA T. Fluid forces on oscillating cylinders[J]. **Journal of Waterway Port Coastal and Ocean Division ASCE,** 1978, 104 (WW4): 275-290.